13th International Conference on
Structural Health Monitoring of Intelligent Infrastructure
DOI: 10.3217/978-3-99161-057-1-087

Development of SFCW Radar System for Concrete Structure Inspection

Sangho Lee [1], Keunhee Cho [1], Ji-Young Choi [1], Joo-Hyung Lee [1], Imjong Kwahk [1], Changbin Joh [1]
[1]Korea Institute of Civil Engineering and Building Technology (KICT), Republic of Korea
email: slee0614@kict.re.kr, kcho@kict.re.kr, legion@kict.re.kr, leejoohyung@kict.re.kr, kwakim@kict.re.kr, cjoh@kict.re.kr

ABSTRACT: Ground Penetrating Radar (GPR) is commonly used for internal inspection of concrete structures. However, the fixed design parameters of commercial GPR limit adaptability for specific inspection conditions and integration with emerging technologies. This study presents the development of a Stepped-Frequency Continuous Wave (SFCW) radar for concrete structure assessment, based on numerical simulations and experimental validation. Parametric analysis was performed to evaluate the influence of frequency bandwidth, antenna spacing, synthetic aperture length, and beamwidth on imaging performance, particularly in detecting embedded reinforcing bars. B-scan data were generated and processed using Delay and Sum Algorithm (DSA) for an image focusing, and image resolution was evaluated in both azimuth and range directions. Based on the simulation results, an SFCW radar prototype was built, and its performance was assessed through tests on reinforced concrete specimens. The experimental results confirmed the system's capability to detect internal targets. The findings suggest that the proposed radar system offers improved flexibility and adaptability for concrete inspection compared to conventional commercial GPR.

KEY WORDS: Nondestructive Estimation; SFCW Radar; GPR; Image Focusing; Concrete Structure Inspection.

1 INTRODUCTION

In recent decades, the deterioration of civil infrastructure has become a growing issue in many countries. In addition, extreme climate events have introduced loading and environmental conditions that were not considered during the original design and construction phases. Under such conditions, accurate structural condition assessment and maintenance technologies are essential. For reinforced concrete structures, identifying internal features such as voids and rebar structure is necessary for reliable performance evaluation. Currently, Ground Penetrating Radar (GPR) is widely used for internal inspection of concrete structures [1, 2, 3, 4, 5]

GPR can be categorized into impulse-type and stepped-frequency continuous wave (SFCW) type depending on the signal transmission method [1]. Impulse-type GPR transmits short-duration electromagnetic pulses, while SFCW GPR transmits continuous waves by sweeping the frequency in discrete steps. SFCW has advantages in terms of signal-to-noise ratio and penetration depth [6], and is also used for concrete inspection applications [7, 8, 9, 10]

The image quality of GPR data depends on various radar design parameters such as waveform, frequency bandwidth, antenna characteristics, and scanning distance (synthetic aperture). These parameters affect the azimuth (scan direction) and range (depth direction) resolution and the overall imaging performance [6, 11]. However, most commercial GPRs have fixed configurations in terms of frequency range, antenna spacing, and polarization, which limits the ability to optimize inspections for specific applications. Additionally, integrating GPR with technologies such as drones or multi-channel antenna arrays is restricted. Therefore, it is necessary to develop a customizable radar platform for concrete inspection.

This study develops an SFCW radar for internal imaging of concrete structures through numerical simulations and experimental validation. The effects of key design parameters - frequency bandwidth, antenna spacing, synthetic aperture length, and beamwidth - on imaging quality were analyzed using simulation. Based on the results, a SFCW radar system was constructed and its performance was evaluated through experimental tests on reinforced concrete specimens.

2 DESIGN OF SFCW RADAR FOR CONCRETE SCAN

2.1 SFCW Radar

An SFCW radar transmits continuous waves while incrementally increasing the frequency from a minimum frequency (f_{min}) to a maximum frequency (f_{max}) at fixed intervals Δf, as expressed in Equation (1) [6]:

$$s_{tx,i}(t) = A_i \cos(2\pi f_i t + \phi_i) \quad (1)$$

Here, $s_{tx,i}(t)$, f_i, A_i, and ϕ_i represent the i-th transmitted wave, its frequency, amplitude, and phase, respectively, and t is time. The received signal is a delayed version of the transmitted signal, with a round-trip delay (τ) due to the wave propagating to and from the target, as shown in Equation (2):

$$s_{rx,i}(t) = B_i \cos(2\pi f_i(t - \tau) + \phi_i) \quad (2)$$

In this equation, $s_{rx,i}(t)$ is the received signal corresponding to the i-th transmission (A-scan), B_i is the attenuated amplitude. Due to spherical spreading and material attenuation, B_i is typically proportional to $(\Delta t/\tau)^2$. Δt is the time step between A-scans. The radar module demodulates the received signal into a baseband signal in frequency domain as in Equation (3):

DOI: 10.3217/978-3-99161-057-1-087

$$S_{f,i} = (\Delta t/\tau)^2 C_i \exp(-j2\pi f_i \tau) \quad (3)$$

Here, C_i is a coefficient related to the amplitude and assumed to be 1. The time domain response is then obtained by applying the inverse Fourier transform to the frequency domain signal:

$$s_{t,m} = \mathcal{IFT}(S_f)_m \quad (4)$$

where m denotes the scan position. Performing this calculation across all scan positions yields the B-scan data.

2.2 GPR Image Focusing

To obtain focused images, image processing is applied to the acquired B-scan data. In this study, the Delay and Sum Algorithm (DSA) was used for image focusing [12]. The focused image $g(x_i, z_j)$ is calculated as:

$$g(x_i, z_j) = \frac{1}{M} \sum_{m \in C_x} s_{t,m}(\tau)$$

where (x_i, z_i) denotes the azimuth and range coordinates of an image pixel, m is the number of A-scan positions, C_x is the set of A-scan positions.

To analyze the design parameters of SFCW radar for concrete inspection, a simulation was performed as illustrated in Figure 1. Two reinforcing bars were embedded 50 mm deep in concrete with a center-to-center spacing of 50 mm. This spacing was chosen based on the maximum aggregate size and typical cover thickness. The relative permittivity of concrete was assumed to be 10 [13], and the rebars were modeled as point targets.

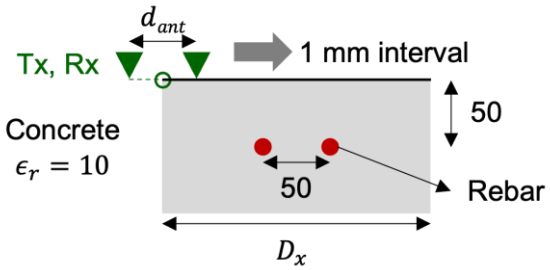

Figure 1. Numerical simulation model (unit: mm)

The frequency bandwidth used in the simulation was set to 1–5 GHz, based on typical GPR configurations for concrete inspection [7]. The transmitting and receiving antennas were placed on the surface of the concrete with a defined spacing, and moved horizontally with 1 mm step intervals to simulate scanning. The antenna was assumed to have a beamwidth (θ), and signals outside this angle were ignored for simplicity.

Figure 2(a) shows a representative B-scan image generated through the simulation (d_{ant} = 80 mm, θ = 120°). The amplitude values were normalized to a range of 0 to 1. The time interval was set to 5 ps, and the total time window was determined to be 20 ns based on the 50 MHz frequency step. Only the reflections from the rebars were considered, and surface reflections and direct waves were excluded, assuming that background removal would eliminate these components [14]. Background removal was performed by averaging the B-scan data along the scan direction and subtracting it from the original signal.

Figure 2(b) shows the focused image obtained by applying DSA to the B-scan in Figure 2(a), also normalized from 0 to 1. The image shows a strong reflection at the rebar locations, with decreasing amplitude as the distance from the rebar increases, indicating that the imaging and focusing were successful.

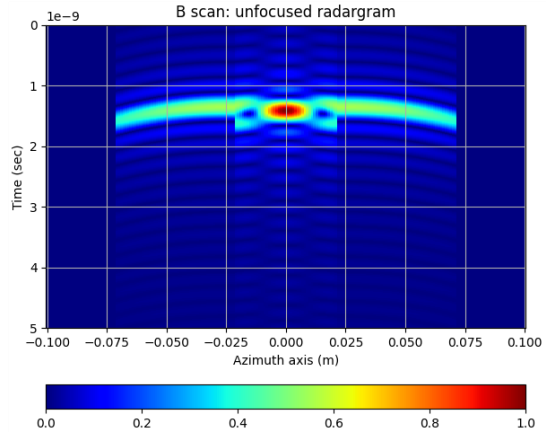

(a) B-scan data

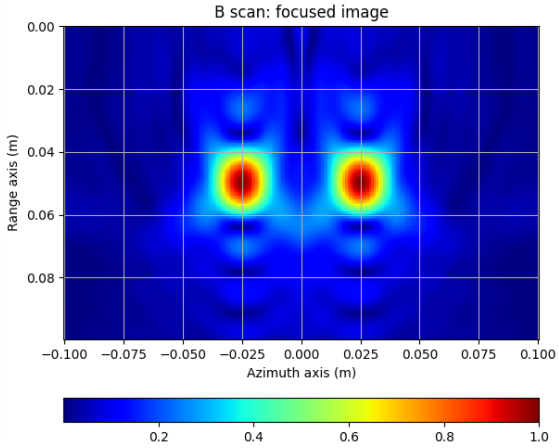

(b) Focused image

Figure 2. Simulation results

Figure 3 shows the reflection amplitude in dB scale along a cross-section including the rebars, and the –3 dB resolution was measured in both azimuth and range directions [15].

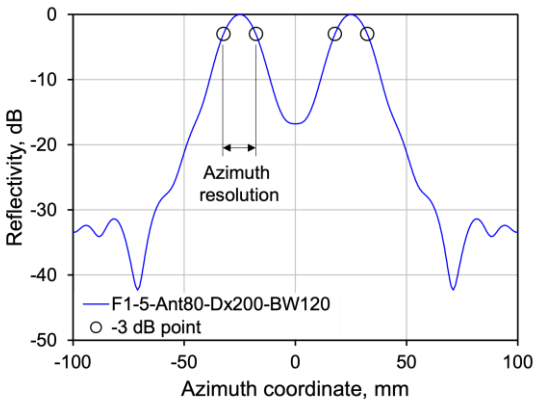

DOI: 10.3217/978-3-99161-057-1-087

(a) Azimuth cross-section

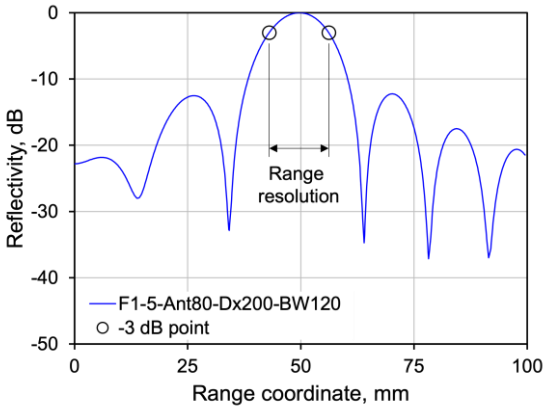

(b) Range cross-section

Figure 3. Distribution of reflectivity at rebar cross section

2.3 SFCW Radar Design Parameters

Based on the numerical simulations, several design parameters for SFCW radar in concrete scanning were considered. First, wide frequency bandwidth is required, and higher frequency components are preferred unless significantly attenuated. Vivaldi antennas, commonly used in wideband applications, can be applied [16]. However, electromagnetic attenuation in concrete increases with frequency [17], so optimal bandwidth selection should consider this trade-off.

Second, a smaller antenna spacing improves resolution, but mutual coupling effects must be considered. The simulation did not account for these effects, but in practice, closely spaced antennas may interfere with each other's radiation patterns and impedance [18,19]. Therefore, antenna spacing should be minimized without causing mutual coupling.

3 SFCW RADAR DEVELOPMENT AND VALIDATION

3.1 Radar Configuration

A vector network analyzer (VNA) is a device used to evaluate the frequency domain performance of RF components by sweeping a wide frequency range. When combined with appropriate antennas, it can function as an SFCW radar. In this study, the UVNA-63, the educational VNA by Mini-Circuits, was used as the SFCW radar module (Figure 4).

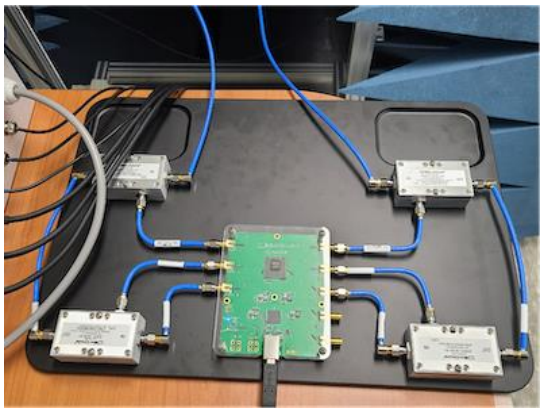

Figure 4. UVNA-63 (https://www.minicircuits.com)

The device provides a maximum output power of 0 dBm and operates in the frequency range from 0.1 to 6 GHz, which covers the frequency range of typical commercial GPRs [8, 9, 10]. The maximum receive input level is 10 dBm.

For transmission and reception, a wideband Vivaldi antenna (113 × 150 mm) was used (https://www.craeca.com/antenna).

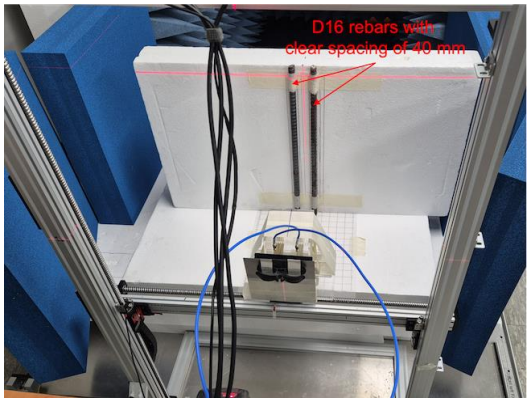

Figure 5. Preliminary test for antenna spacing

As shown in Figure 5, the antenna was mounted on a 2D motorized scanning frame that enables C-scan acquisition. The horizontal scan range was set to 1150 mm to secure a sufficient synthetic aperture length. This configuration ensures that concrete members located 100 mm away can be scanned up to approximately 1.2 m in depth. The antennas were oriented so that the scan direction aligned with the H-plane, which typically has a wider beamwidth. The antenna used in this study had a reduced beamwidth at higher frequencies, indicating the need for further development of antennas that maintain beamwidth across the full frequency range.

A preliminary experiment was conducted to determine the appropriate antenna spacing using two D16 rebars (SD400 grade) placed 40 mm apart in air, as shown in Figure 5. The antennas were spaced at 9, 50, and 88 mm during horizontal B-scan. The rebars were positioned 165 mm away from the antenna tips and fixed using Styrofoam, which has a relative permittivity of approximately 1.04 [20], making it nearly equivalent to air and minimally affecting the measurement. Electromagnetic absorbers were placed around the rebars to minimize environmental reflections.

The transmission bandwidth was set to 1–5 GHz based on antenna performance, with 50 MHz frequency steps. The transmit power was 0 dBm. A-scan data were acquired at 2 mm intervals over a scan distance of 600 mm. To enhance high-frequency components in the measured data, an amplification process was applied as defined in Equation (6), where R was empirically set to 1000:

$$S_{enchanced,i} = S_{f,i} \exp\left[\ln R \frac{f_i - f_{min}}{f_{max} - f_{min}}\right] \quad (6)$$

Here, $S_{enchanced,i}$ is the amplified signal at frequency f_i, and f_{min} and f_{max} are the minimum and maximum frequencies, respectively.

The B-scan data were processed with background removal and DSA for image focusing. Figure 6 shows the experimental results. The white circles indicate the positions of the rebars.

DOI: 10.3217/978-3-99161-057-1-087

Unlike the simulation results, lower resolution was observed when the antennas were placed too close together. At 9 mm spacing, the two rebars could not be distinguished. When the spacing was increased to 88 mm, the rebars were clearly resolved. This result indicates that at least 88 mm of antenna separation is required to suppress mutual coupling effects.

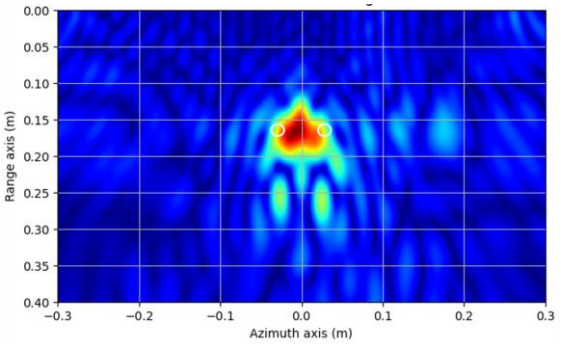

(a) Antenna spacing 9 mm

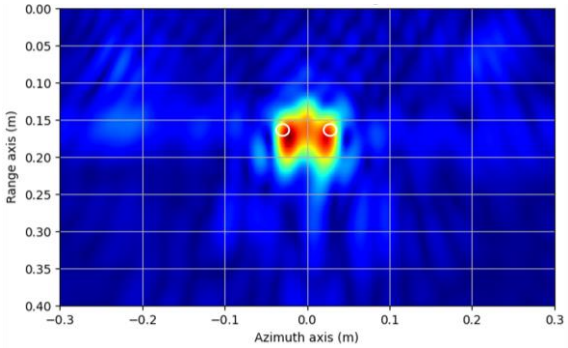

(b) Antenna spacing 50 mm

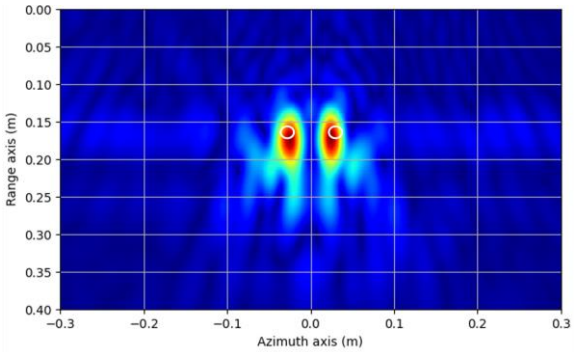

(c) Antenna spacing 88 mm

Figure 6. Preliminary test results

3.2 Validation Test

To validate the developed SFCW radar, an experiment was conducted using a reinforced concrete specimen. Figure 7 shows the geometry of the specimen. The concrete block measured 160 × 200 × 260 mm and included six D16 rebars (SD400) embedded in two layers. The vertical spacing between the two layers was 50 mm, and the horizontal spacing between rebars in the same layer was 50 mm and 70 mm. The compressive strength of the concrete was 30 MPa, a typical value for structural applications. The antenna spacing was set to 100 mm to avoid mutual coupling effects. The scan length was 1000 mm with 2 mm measurement intervals. The standoff distance between the antenna and the specimen surface was 100 mm. The same high-frequency amplification process used in the preliminary test was applied to the acquired data.

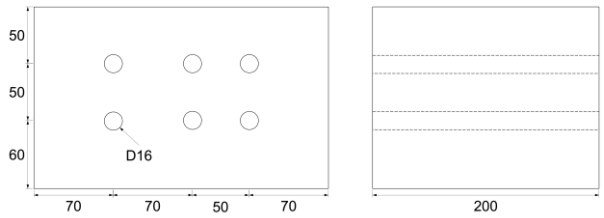

Figure 7. Concrete test specimen (unit: mm)

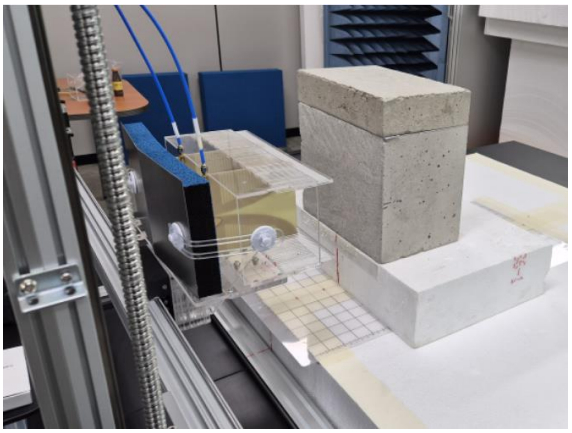

Figure 8. Verification test setup

Figure 8 shows the experimental setup. To minimize environmental interference, only the concrete specimen was placed in the direction of wave propagation. The scan was performed on the surface with a concrete cover of 42 mm. The transmit frequency range was set from 0.1 to 6 GHz in 50 MHz steps, and the transmit power was 0 dBm.

The acquired B-scan data were processed using background removal and DSA. Figure 9(a) shows the time-domain B-scan after high-frequency amplification and background removal. A strong surface reflection was observed due to the large area of the concrete surface, exceeding the strength of the rebar reflections. DSA was applied with a relative permittivity of 7 for concrete. Refraction at the air–concrete interface was accounted for using Snell's law. Figure 9(b) shows the focused image in dB scale for the scan area (260 mm in azimuth, 160 mm in range). Strong reflections were observed at the positions of the front-layer rebars, and three distinct rebar signatures were clearly identified. The positions in both range and azimuth directions matched the actual locations of the rebars. These results confirm that the developed radar can detect and localize rebars located 50 mm deep in concrete.

However, the rebars in the rear layer were not detected in the focused image. This is attributed to signal attenuation during propagation and interference from surface and front-layer reflections. Since the rear-layer signal becomes weaker and is partially masked by stronger reflections, detection is more difficult. To address this, future research is required on signal compensation techniques, clutter removal methods, and

DOI: 10.3217/978-3-99161-057-1-087

antenna design that enhances high-frequency transmission for deeper penetration.

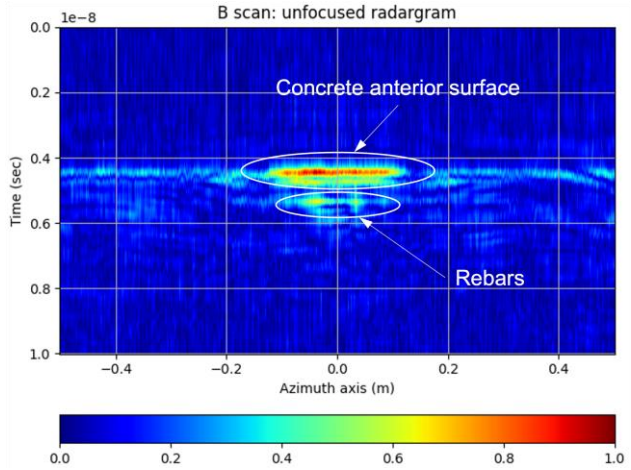

(a) B-scan data

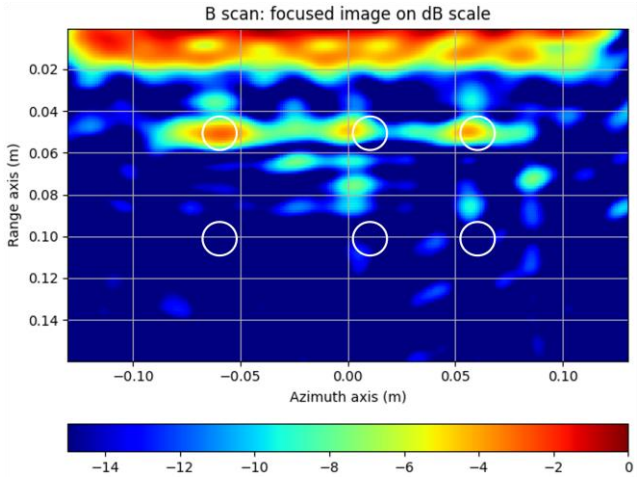

(b) Focused image

Figure 9. Verification of test result

4 CONCLUSION

This study conducted numerical simulations and experimental tests to develop an SFCW radar system for internal inspection of concrete structures. The following conclusions were drawn:

1. To analyze the effects of SFCW radar design parameters on image quality, simulations and image focusing were performed using rebar-embedded concrete models. The results identified five key design parameters for an SFCW radar in concrete scanning:

(1) A wide frequency bandwidth is required, and higher frequency components should be used as long as attenuation is acceptable.

(2) The antenna spacing should be minimized without introducing mutual coupling effects.

(3) The synthetic aperture length should exceed the expected rebar spacing and target area.

(4) A larger antenna beamwidth improves resolution; therefore, the antenna should be oriented such that the scan direction aligns with the plane having a wider beam.

(5) Amplifying high-frequency components while maintaining overall bandwidth improves azimuth resolution without degrading range resolution.

2. An SFCW radar system was developed using a vector network analyzer. Ultra-wideband Vivaldi antennas were employed. Preliminary tests were conducted on exposed rebar with varying antenna spacing. The results showed that mutual coupling effects were avoided when the spacing was 88 mm or more.

3. A validation experiment was conducted on a reinforced concrete specimen using the developed radar. The focused image showed strong reflections at the locations of the front-layer rebars, and three rebars were clearly detected. This confirmed the radar's ability to identify and localize rebars embedded 50 mm deep in concrete. However, the rear-layer rebars were not detected due to signal attenuation and masking by front-layer reflections. To address this, further research is needed on signal compensation, clutter suppression, and antenna design for improved high-frequency transmission.

The developed SFCW radar offers greater flexibility than commercial systems, as its configuration can be freely modified by the user. This advantage makes it suitable for structure-specific inspection applications, integration with emerging technologies such as UAVs, multi-channel antenna arrays, and the development of new NDT techniques. With continued development, the proposed system has the potential to outperform existing commercial GPRs in terms of performance and applicability.

ACKNOWLEDGMENTS

Research for this paper was carried out under the KICT Research Program (project no. 20250057-001, Concrete CT: Reinforcement Damage) funded by the Ministry of Science and ICT.

REFERENCES

[1] ACI Committee 228, Report on nondestructive test methods for evaluation of concrete in structures (ACI 228.2R-13), American Concrete Institute, Farmington Hills, MI, USA, 2013.

[2] J.E. Baek, H.J. Lee, K.C. Oh, and B.S. Eom, "Evaluation of Concrete Bridge Deck Deterioration Using Ground Penetrating Radar Based on an Extended Common Mid-Point Method," *J. Korea Inst. Struct. Maint. Inspect.*, vol. 16, no. 6, pp. 82–92, 2012. (In Korean)

[3] E.J. Kim, S.J. Cho, and S.H. Sim, "A Recent Research Summary on Smart Sensors for Structural Health Monitoring," *J. Korea Inst. Struct. Maint. Inspect.*, vol. 19, no. 3, pp. 10–21, 2015. (In Korean)

[4] J. Rhee, J. Shim, S. Lee, and K.H. Lee, "A Consideration on the Electromagnetic Properties of Road Pavement Using Ground Penetrating Radar (GPR)," *KSCE J. Civil and Environmental Engineering Research*, vol. 40, no. 3, pp. 285–294, 2020. (In Korean)

[5] C. Ozdemir, Ş. Demirci, E. Yiğit, and B. Yilmaz, "A review on migration methods in B-scan ground penetrating radar imaging," *Mathematical Problems in Engineering*, vol. 2014, p. 280738, 2014.

[6] C. Nguyen and J. Park, *Stepped-Frequency Radar Sensors: Theory, Analysis and Design*, Springer, Cham, Switzerland, 2016.

[7] D. Huston, J.O. Hu, K. Muser, W. Weedon, and C. Adam, "GIMA ground penetrating radar system for monitoring concrete bridge decks," *Journal of Applied Geophysics*, vol. 43, pp. 139–146, 2000.

[8] T. Lee, M. Kang, M. Choi, S.E. Jung, and H. Choi, "Development of Thickness Measurement Method From Concrete Slab Using Ground Penetrating Radar," *J. Korea Inst. Struct. Maint. Inspect.*, vol. 26, no. 3, pp. 39–47, 2022. (In Korean)

[9] H.J. Lim, "Application of Ground Penetrating Radars (GPR) in Concrete Bridges: A Review," *Journal of the Korea Concrete Institute*, vol. 36, no. 4, pp. 329–336, 2024. (In Korean)

DOI: 10.3217/978-3-99161-057-1-087

[10] S. Park, J. Kim, W. Kim, H. Kim, and S. Park, "A Study on the Prediction of Buried Rebar Thickness Using CNN Based on GPR Heatmap Image Data," *J. Korea Inst. Struct. Maint. Inspect.*, vol. 23, no. 7, pp. 66–71, 2019. (In Korean)
[11] C. Ozdemir, Inverse Synthetic Aperture Radar Imaging with MATLAB Algorithms, John Wiley & Sons, Hoboken, NJ, USA, 2021.
[12] M. Schickert, M. Krause, and W. Muller, "Ultrasonic Imaging of Concrete Elements Using Reconstruction by Synthetic Aperture Focusing Technique," *Journal of Materials in Civil Engineering*, vol. 15, no. 3, pp. 235–246, 2003.
[13] D.H. Chen and A. Wimsatt, "Inspection and Condition Assessment Using Ground Penetrating Radar," *Journal of Geotechnical and Geoenvironmental Engineering*, vol. 136, no. 1, pp. 207–214, 2010.
[14] D.J. Clem, T. Schumacher, and J.P. Deshon, "A consistent approach for processing and interpretation of data from concrete bridge members collected with a hand-held GPR device," *Construction and Building Materials*, vol. 86, pp. 140–148, 2015.
[15] M.A. Tolman, A Detailed Look at the Omega-k Algorithm for Processing Synthetic Aperture Radar Data, Master's Thesis, Brigham Young University, Utah, USA, 2008.
[16] A.M.D. Oliveira, M.B. Perotoni, S.T. Kofuji, and J.F. Justo, "A Palm Tree Antipodal Vivaldi Antenna With Exponential Slot Edge for Improved Radiation Pattern," *IEEE Antennas and Wireless Propagation Letters*, vol. 14, pp. 1334–1337, 2015.
[17] S. Kim, J. Surek, and J. Baker-Jarvis, "Electromagnetic metrology on concrete and corrosion," *Journal of Research of the National Institute of Standards and Technology*, vol. 116, no. 3, pp. 655–669, 2011.
[18] R.G.S. Alsultan and G.O. Yetkin, "Mutual Coupling Reduction of E-Shaped MIMO Antenna with Matrix of C-Shaped Resonators," *International Journal of Antennas and Propagation,* vol. 2018, no. 1, p. 4814176, 2018.
[19] C.A. Balanis, *Antenna Theory: Analysis and Design*, 3rd ed., John Wiley & Sons, Hoboken, NJ, USA, 2005.
[20] M. Plonus, "Theoretical investigations of scattering from plastic foams," *IEEE Transactions on Antennas and Propagation*, vol. 13, no. 1, pp. 88–94, 1965.